AG5 is a potent non-steroidal anti-inflammatory and immune regulator that preserves innate immunity

Pablo Botella-Asunción [a,*], Eva M. Rivero-Buceta [a], Carla Vidaurre-Agut [a], Raquel Lama [b], Magalí Rey-Campos [b], Alejandro Moreno [b], Laura Mendoza [c], Patricia Mingo-Casas [d], Estela Escribano-Romero [d], Alfonso Gutierrez-Adan [e], Juan Carlos Saiz [d], Cristian Smerdou [f], Gloria Gonzalez [f], Felipe Prosper [g], Josepmaría Argemí [g], Jesus San Miguel [g], Pedro J. Sanchez-Cordón [h], Antonio Figueras [b], Jose Manuel Quesada-Gomez [i], Beatriz Novoa [b], María Montoya [c], Miguel A. Martín-Acebes [d], Antonio Pineda-Lucena [j], Jose María Benlloch [k,*]

[a] *Institute of Chemical Technology (ITQ), Universitat Politècnica de Valencia-Spanish National Research Council (CSIC), 46022 Valencia, Spain*
[b] *Institute of Marine Research (IIM), Spanish National Research Council (CSIC), 36208 Vigo, Spain*
[c] *Molecular Biomedicine Department, BICS Unit, Centro de Investigaciones Biológicas Margarita Salas (CIB), Spanish National Research Council (CSIC), 28040 Madrid, Spain*
[d] *Department of Biotechnology, Instituto Nacional de Investigación y Tecnología Agraria y Alimentaria, Spanish National Research Council (CSIC), 28040 Madrid, Spain*
[e] *Animal Reproduction Department, Instituto Nacional de Investigación y Tecnología Agraria y Alimentaria, Spanish National Research Council (CSIC), 28040 Madrid, Spain*
[f] *DNA & RNA Medicine Division, Centro de Investigación Medica Aplicada (CIMA), Universidad de Navarra, 31008 Pamplona, Spain*
[g] *Hematology Service and Cell Therapy Unit and Program of Hematology-Oncology CIMA-Universidad de Navarra, Cancer Center Clínica Universidad de Navarra (CCUN) and Instituto de Investigación Sanitaria de Navarra (IdISNA), Pamplona, Spain. Centro de Investigación Biomedica en Red Cancer (CIBERONC) and RICORS TERAV, Madrid, Spain*
[h] *Veterinary Pathology Unit, Animal Health Research Center (CISA), Instituto Nacional de Investigación y Tecnología Agraria y Alimentaria, Spanish National Research Council (CSIC), 28130 Madrid, Spain*
[i] *Maimonides Biomedical Research Institute of Cordoba (IMIBIC), Hospital Universitario Reina Sofía, 14004 Córdoba, Spain*
[j] *Enabling Technologies Division, Centro de Investigación Medica Aplicada (CIMA), Universidad de Navarra, 31008 Pamplona Spain*
[k] *Institute of Instrumentation for Molecular Imaging (I3M), Universitat Politècnica de Valencia-Spanish National Research Council (CSIC), 46011 Valencia, Spain*

ARTICLE INFO

ABSTRACT

An archetypal anti-inflammatory compound against cytokine storm would inhibit it without suppressing the innate immune response. AG5, an anti-inflammatory compound, has been developed as synthetic derivative of andrographolide, which is highly absorbable and presents low toxicity. We found that the mechanism of action of AG5 is through the inhibition of caspase-1. Interestingly, we show with in vitro generated human monocyte derived dendritic cells that AG5 preserves innate immune response. AG5 minimizes inflammatory response in a mouse model of lipopolysaccharide (LPS)-induced lung injury and exhibits in vivo anti-inflammatory efficacy in the SARS-CoV-2-infected mouse model. AG5 opens up a new class of anti-inflammatories, since contrary to NSAIDs, AG5 is able to inhibit the cytokine storm, like dexamethasone, but, unlike corticosteroids, preserves adequately the innate immunity. This is critical at the early stages of any naïve infection, but particularly in SARS-CoV-2 infections. Furthermore, AG5 showed interesting antiviral activity against SARS-CoV-2 in humanized mice.

1. Introduction

The pandemic of coronavirus 19 disease (COVID-19), caused by the severe acute respiratory syndrome coronavirus (SARS-CoV)− 2, is the greatest challenge ever faced by modern medicine and public health systems worldwide. From the earliest descriptions it was clear that the high morbidity and mortality was due to dysregulation of the innate immune system leading to an exuberant pro-inflammatory cytokine and

chemokine response causing acute respiratory distress syndrome, with systemic inflammation, septic shock, and multi-organ failure [1]. In a large non-anonymized randomized clinical trial (RECOVERY), low-dose dexamethasone decreased mortality in patients receiving invasive mechanical ventilation or oxygen alone, but not in those not requiring ventilatory support [2]. Early initiation of corticosteroid therapy was also associated with a higher 28-day mortality rate [3]. Systematic reviews and meta-analysis conducted to evaluate the effect of corticosteroids in patients with mild COVID-19 concluded that the administration of corticosteroids in patients with COVID-19 not requiring oxygen was harmful [4]. This effect of glucocorticosteroids early in the disease appears to be due to the weakening of innate antiviral immunity, resulting in delayed viral clearance and adverse outcomes in severe viral pneumonias [5–7]. Nonetheless, the use of anti-inflammatory drugs in COVID-19 is a valuable therapeutic strategy, and anti-inflammatory drugs are currently at the top of the list of repurposed drugs for the treatment of patients with moderate to severe COVID-19 [8].

Therefore, the aim of this study is to develop a low-toxicity anti-inflammatory compound that, like glucocorticosteroids, would control the cytokine/chemokine storm, but would allow the innate immune system to respond to viral, bacterial, or parasitic infections. Such a compound would be more of an immunomodulatory agent than a mere inhibitor of the entire immune system.

A shortcut to develop a new drug is to use the derivative of a natural compound, which originally has been used for centuries in traditional medicine. Hence, this strategy could increase the probability of avoiding toxicity. We selected andrographolide, the active principle of the *Andrographis paniculata* plant, endemic of certain regions in India, Sri Lanka, and other areas in South East Asia to start a systematic study of different synthetic derivatives. Andrographolide is a diterpenoid lactone anti-inflammatory agent widely used in clinical practice in Asian countries, even though its oral biodisponibility is limited due to huge first-pass metabolism and low water solubility [9].

In the context of respiratory diseases, andrographolide has clinically shown ability to reduce pro-inflammatory mediators release such as NO, IL-1β and IL-6, as well as prostaglandins PGE2 and TXB2 and the allergic mediator LTB4 without antihistamine effect, contributing to improve symptoms in patients with respiratory infections [10]. Andrographolide, unlike corticosteroids, does not inhibit the adrenocortical axis, has no adverse effects on bone or muscle and does not interfere with carbohydrate or lipid metabolism. The metabolism of andrographolide is not completely elucidated, but according to urine analysis [11] and studies in human liver microsomes [12], it seems that regioselective glucoronidation is the most important metabolic route in humans for andrographolide transformation after incorporation to systemic circulation, leading to mostly inactive compounds. Conversely, andrographolide sulfonation is a minor transformation pathway in humans, whereas in rats is the most important metabolism pathway [13,14]. From a therapeutic point of view, the sulfonic derivative presents significant advantages, as it is expected to notably increase the anti-inflammatory activity, also improving the pharmacokinetic profile with regard to the original chemical [14–16]. For this reason, a preliminary short screening in a series of andrographolide derivatives was performed. They were all synthesized and tested within an inflammatory scenario associated to viral infections, by determining IL-6 expression in a transgenic zebrafish larvae model infected with Spring Viremia of Carp Virus (SVCV), from which 14-deoxy-12(R,S)-sulfoandrographolide (named AG5) was selected as the most valuable compound. Subsequently, we evaluated by in vitro testing AG5 anti-inflammatory mechanism and immunomodulatory activity, followed by an in vivo therapeutic study of AG5 anti-inflammatory action in two mouse models, lipopolysaccharide (LPS)-induced lung injury study, and SARS-CoV-2 infection study. Finally, we have determined the toxicological profile of this novel drug in different animal models.

2. Materials and methods

2.1. Materials

Complete description of chemical reagents, cell lines, virus and experimental animals used in this work is provided at the Supporting Information.

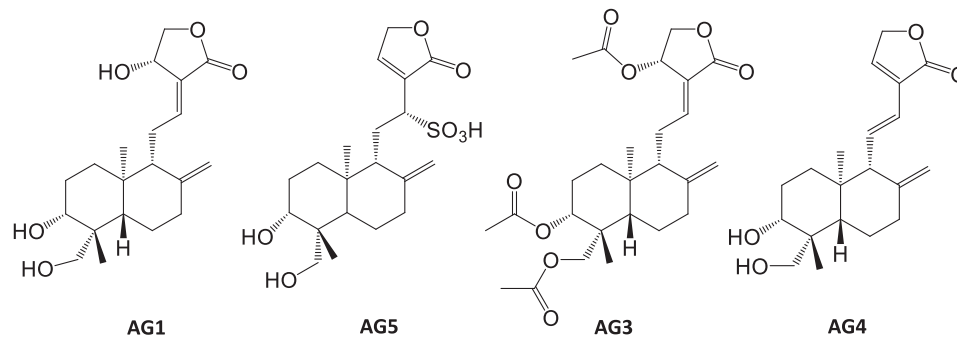### 2.2. Synthesis of andrographolide derivatives

14-deoxy-12(R,S)-sulfo-andrographolide (AG5) has been synthesized, purified and characterized starting from andrographolide (Fig. 1 and Fig. S1). Scaling up preparation process into a Technical Batch has been carried out by GalChimiApplus chemical company (Bellaterra, Spain). Briefly, andrographolide (10 g) was dissolved in 200 mL of 95% ethanol on heating at reflux (1 h, to ensure complete dissolution of the andrographolide) (solution 1). To 40 mL of Na_2SO_3 1 M, 48 mL of 2% H_2SO_4 (wt/wt) and 80 mL of water was added (solution 2). Solution 1 (at 75 ºC) was poured into solution 2 (at 75ºC) and refluxed for one hour. The reaction solution was allowed to cool up to room temperature. The pH value of the reaction solution was adjusted to 6–7 by adding 2% H_2SO_4 (v/v), and the solution was led to dryness in a rotary evaporator under reduced pressure (67 mbar) and water bath (60 ºC). Subsequently, the residue was dissolved with 100 mL water, followed by a three-fold extraction with same chloroform volume (3 ×100 mL). Then, the isolated aqueous layer was evaporated to dryness in a rotary evaporator (67 mbar, 60º C). This residue was re-dissolved in 100 mL of methanol and filtered using a Buchner Funnel Vacuum Filtration with a Whatman filter paper 42. The supernatant was evaporated to dryness in a rotary evaporator (337 mbar, 60º C), freeze-dried (−55 ºC, 16 h) and finally purified by High Performance Flash Chromatography (HPFC) in a Biotage® Selekt unit, by using a reversed-phase column (Biotage® Sfär C18 D Duo 100 Å 30 μm 120 g). Separation of the pure compound was carried out with acetonitrile 100% (250 mL/min, 45 min). The recovered liquid phase was evaporated under reduced pressure (223 mbar, RT) and finally freeze-dried (−55 ºC, 16 h), yielding a white powder (14-deoxy-12(R,S)-sulfo andrographolide, yield = 30–35%). Characterization is provided at the Supporting Information.

The synthesis and characterization of the other andrographolide derivatives, 3,14,19-Triacetylandrographolide (AG3, Fig. 1B) and 14-Deoxy-11,12-Didehydroandrographolide (AG4, Fig. 1C) is provided at the Supporting Information.

2.3. In vitro validation of AG5 anti-inflammatory activity

2.3.1. Inhibition of caspase-1 by AG5

In other to determine the intracellular AG5 anti-inflammatory mechanism, THP-1 monocyte cells (American Type Culture Collection, ATCC, USA) were seed into 24-wells cell culture plates with 0.5 mL of cell suspension in each well (10^6 cells/mL). THP-1 is a human leukemia monocytic cell line, which has been extensively used to study monocyte/macrophage functions, mechanisms, signaling pathways, as well as nutrient and drug transport. This cell line has become a common model to estimate modulation of monocyte and macrophage activities. This is very relevant in the case of studying responses in the innate immune system [17]. Differentiated cells were pre-treated during 1 h with the andrographolide or AG5 (10 μM) and then stimulated with LPS (100 ng/mL). After 2 h, a second stimulus was added, ATP (5 mM) for 1 h. Untreated and unstimulated controls were also included. Caspase-Glo 1 Inflammasome Assay kit (Promega) was used to determine the ability of andrographolide and AG5 to modify the activity of the enzyme caspase-1. This activity was tested in the supernatant of differentiated THP-1 cells treated and stimulated as described above. The Z-WEHD substrate was reconstituted to prepare the Caspase-Glo 1 Reagent and MG-132 inhibitor (a proteasome inhibitor) was added to a final concentration of 60 μM in the assay. The half of this mixture was

Fig. 1. Chemical structure of andrographolide derivatives. AG1: andrographolide. AG5: 14-deoxy-12(R,S)-sulfo-andrographolide. AG3: 3,14,19-triacetylandrographolide. AG4: 14-deoxy-11,12-didehydroandrographolide.

transfer to a separate tube, and the Ac-YVAD-CHO inhibitor (a selective inhibitor of the enzyme caspase-1) at a final concentration of 1 μM was added. Before starting the assay, the reagents were equilibrated to room temperature. Cell culture medium from each well of the experimental plate (50 μL) was transferred to a white 96-well plate and Caspase-Glo 1 reagent was immediately added (50 μL) to a half of the wells containing the transferred culture medium, in the other half of the plate containing the same samples, the Caspase-Glo 1 YVAD-CHO reagent was added to confirm the caspase-1 activity. The plate was incubated at room temperature for 1 h for the luminescent signal to stabilize and measures were made every 30 min for 3 h using the GloMax Discover Microplate Reader (Promega). The measurements of blank wells were subtracted from the rest of the experimental wells. Released IL-1β cytokine was determined in the supernatants by Enzyme Linked-Immuno-Sorbent Assay (ELISA, see Supporting Information). Three independent experiments were performed, with 3 biological replicates.

2.3.2. AG5 modulation of immune response

Human monocyte derived dendritic cells (moDC) were plated with the required stimuli at the following concentrations: LPS (1 μg/mL) or Poly (I:C) (30 μg/mL). After 1 h, AG-5 (10 μM) or dexamethasone (10 μM) were added. Untreated and unstimulated controls were also included. Released cytokines after 24 h treatment were analysed in supernatants by ELISA. Three independent experiments with 3 biological replicates were performed.

2.4. In vivo validation of AG5 anti-inflammatory activity

2.4.1. Validation in transgenic zebrafish model

We carried out a preliminary short screening in a series of andrographolide derivatives synthesized and tested for treatment of inflammatory disease associated to viral infection, by determining IL-6 expression in zebrafish larvae model infected with SVCV. For comparative purpose, the parent andrographolide (AG1) was also tested. Fish care and challenge experiments were reviewed and approved by the CSIC National Committee on Bioethics. Bath concentration of andrographolide and derivatives was adjusted according to their water solubility pattern: AG1, AG3 5 μM; AG4, AG5 10 μM. For microinjection experiments, larvae were anesthetized by adding two drops of a 0.05% MS-222 solution to a Petri plate with a volume of 10 mL of water. Zebrafish were euthanized using a MS-222 overdose (500 mg/l^{-1}). The infections of larvae with SVCV were conducted by microinjection in the duct of Cuvier (2 nL of SVCV suspension, 5×10^4 TCID50/mL). Zebrafish larvae at 2 days post fertilization (dpf) were firstly treated with andrographolide derivatives by bath during 96 h, using 6-well plates with 14 larvae/well (3 biological replicates), and no toxicity (e.g., larvae mortality) was observed in any case. Subsequently, zebrafish larvae at 3 dpf were treated with andrographolide derivatives by bath during 24 h and then infected with SVCV or treated with culture medium. After 24 h larvae were harvested to analyse the viral replication and the expression

levels of IL-6 gen by one-step quantitative real-time polymerase chain reaction (RT-qPCR). The experiment was done in triplicate, with 4 biological replicates and 5 larvae/replicate).

To further understand the effects of AGs in inflammation we used a zebrafish model of inflammation resolution, in which neutrophils can be followed in transparent larvae during the resolution phases of inflammation following tissue injury or an infection. For this purpose, Tg(*lyz*: DsRed2) transgenic larvae (3 dpf) were microinjected in the duct of Cuvier with 2 nL of a solution with SVCV and the corresponding andrographolide derivative for the infected and treated groups, SVCV and PBS for the infected and untreated groups, or cell medium and PBS for the uninfected and untreated groups. After 2 h of this microinjection, images of whole larvae were taken. Two different experiments were carried out, with 8 larvae/group.

Moreover, we also evaluated the anti-inflammatory effects of andrographolide and derivatives in the transgenic line Tg(*mpx*:GFP). Briefly, at 3 dpf the tails were cut with a razor and then the larvae were immersed in water containing the corresponding andrographolide derivative for the treated groups and or without them for the control groups. The resolution of neutrophilic inflammation was assessed counting neutrophils (GFP+ cells) number after 24 h at the site of injury. The experiment was done in duplicate, with 8 larvae/group.

Larvae images were taken in a Nikon AZ100 fluorescence microscope. Larvae were anaesthetized with a 0.01% of MS-222 solution. The immune cells labelled (LYZ+ cells) in the transgenic line were counted using a macro of ImageJ program, whereas neutrophil migration to the regenerative tissues was determined after 24 h and photographed with a Nikon DS-Fi1 digital camera. Additional features of zebrafish testing, viral load quantitation and cytokine determination are provided at the Supporting Information.

2.4.2. Validation in a mouse model of LPS-induced lung injury

A total of 60 male BALB/c weighing 21 ± 1 g (7 ± 1 week-old) were used; the animals were divided into groups of 12 each (n = 12). All animals, except mice in the sham control group, received LPS in sterile PBS (~80 μg/kg, 2 μg in 20 μL per mouse), which was given IT under anesthesia by 2 – 3% isoflurane. The animals in sham control group received PBS instillation (20 μL/mouse) without LPS challenge. AG5 was formulated in phosphate buffered saline (PBS), pH 7 at 3 and 6 mg/ mL for intravenous (IV) administration. Dexamethasone was dissolved in DMSO/Solutol® HS-15/PBS (5/5/90, v/v/v) at 0.5 and 1 mg/mL for IV administration. AG5 or Dexamethasone, alone or in combination, was administered IV at 0 h (right after LPS challenge), and at 24, 48 and 72 h after LPS (four doses). The dosing volume was 10 mL/kg for IV route. At 76 h after LPS challenge (4 h after the last administration), the animals were humanly euthanized. Blood and BALF samples were taken for cytokine quantitation by ELISA (see Supporting Information) from half of the mice in every group (mice# 1–6). For the other half of the animals in each group (mice# 7–12), whole lungs (5 lobes) were harvested and kept in 4% formalin for histopathology.

2.4.3. Validation in the SARS-CoV-2-infected mouse model

Experimental infections were performed in the biosafety level 3 (BSL-3) facilities at Centro de Investigación en Sanidad Animal at Instituto Nacional de Investigación y Tecnología Agraria y Alimentaria (CISA, INIA-CSIC). A total of 23 six-week old heterozygote female mice from INIA-CSIC colony of humanized transgenic mice, expressing the human angiotensin-converting enzyme 2 (hACE2) under the control of the human cytokeratin 18 (K18-hACE2) in a C57/BL6 genetic background [18], were used. Animals (n = 5–6) were anesthetized under isoflurane and inoculated daily with a single dose of 30 mg/kg AG-5 (IV by retro-orbital injection), 50 mg/kg remdesivir twice per day (s.c.), AG-5 and remdesivir, or drug vehicles as a control. Treatment started 2 h before infection. For infections, animals were anesthetized under isoflurane an infected intranasally (i.n.) with 5×10^4 plaque-forming units (pfu) of SARS-CoV-2 D614G isolate hCoV-19/Spain/SP-VHIR.02, D614G(S). This dosage of SARS-CoV-2 was selected on the basis of our previous experiments as it induced extensive expression of proinflammatory cytokines in the lungs and results in high lethalithy in K18-hACE2 infected-mice [18,19]. A prophylactic dose of AG5 (30 mg/kg) was intravenously administered 2 h before virus challenge followed by continued dosing once per day (QD) for 3 more days. Remdesivir dose was given twice a day (BID) by subcutaneous injection and maintained until second day post-infection (dpi), as described [20]. Animals were monitored daily for weight and clinical signs. Mice were euthanized 3 h after the last dose. Furthermore, in order to emulate the standards of care in COVID-19, another group received AG5 (30 mg/kg) in combination with the antiviral remdesivir (50 mg/kg) [21,22]. Control groups were treated with vehicle or remdesivir. After end point, mouse right lungs were harvested, for quantification of viral load and released cytokines by RT-qPCR (see Supporting Information). Moreover, the entire left lung was removed from each K18-hAC2 mouse and immersion-fixed in 4% buffered formalin solution for 48 h for the histopathological study.

2.4.4. Lung histopathological analysis

The histopathological examination was carried out according to standard techniques, and the severity of lung lesions was graded according to described methods [23,24]. Lungs were removed from each mouse and immersion-fixed in 4% buffered formalin solution. After fixation period, samples were routinely processed and embedded in paraffin blocks that were then sectioned at 4 μm thickness on a microtome, mounted onto glass slides and routinely stained with hematoxylin and eosin (H&E). To assess the presence and severity of histopathological lesions, lung inflammation parameters based on previous reports on SARS-CoV-2 infection in mouse models were used [24]. The histopathological parameters evaluated were the follows: alveolar haemorrhages; alveolar oedema; perivascular oedema; alveolar septal thickening (interstitial pneumonia); inflammatory cell infiltration in alveoli; bronchi/bronchioles with epithelial necrosis, detached epithelium or inflammatory cells in the lumen (bronchitis/bronchiolitis); peribronchial/peribronchiolar and perivascular mononuclear infiltrates; cytopathic effect in pneumocytes or syncytia; pleural thickening. The histopathological parameters were graded following a semi-quantitative scoring system as follows: (0) no lesion; (1) minimal lesion; (2) mild lesion; (3) moderate lesion; (4) severe lesion. The cumulative scores of histopathological lesions provided the total score per animal. In each experimental group, the individual scores were used to calculate the group average. In addition, H&E-stained sections were visually scored 0–6 based on the percentage of lung area affected by inflammatory lesions as follows: 0% of the lung injured (score 0); < 5% of the lung injured (score 1); 6–10% (score 2); 11–20% (score 3); 21–30% (score 4); 31–40% (score 5); more than 40% of the lung injured (score 6). In each experimental group, the individual scores were used to calculate the group average. All values represent mean ± SEM in individual groups.

2.5. AG5 toxicological profile

2.5.1. Intrinsic clearance of AG5 in hepatocytes

In order to validate the animal models used in the AG5 toxicology study, which allows translating the preclinical results into the clinical use, we carried out a comparative study in human (mix gender), rat (Sprague-Dawley) and rabbit (New Zealand White) cryopreserved hepatocytes through determination of the intrinsic clearance, according to standard techniques [25]. Three independent experiments with 3 biological replicates were carried out. Additional experimental details can be found at the Supporting Information.

2.5.2. AG5 in vivo toxicological profile in rat and rabbit model

AG5 toxicological preclinical profile under good laboratory practices (GLP) was evaluated according to ICH guideline M3 (R2) over rat (Wistar, 19 females and 15 males) and rabbit (New Zealand, 4 female and 4 male), at the facilities of Drug Development Unit of the Universidad de Navarra (DDUNAV, Pamplona, Spain). All procedures were approved by the Ethical Committee for Animal Experimentation of the University of Navarra and carried out in accordance with the ethical protocol CEEA 001–20. The studies were planned in two phases: a first phase (Phase I) in which the dose administered was increased or decreased depending on the results of morbidity of the previous animal; and a second phase (Phase II) in which specific doses were administered daily for one week in a larger number of animals and in both sexes. Additional description of the toxicological study is provided at the Supporting Information.

2.6. Statistical analysis

All calculations for in vitro testing were performed using one-way ANOVA analysis and a Bonferroni test correction was applied. Data were compared two by two, using repeated measures for each condition. For the preliminary study in transgenic zebrafish model, gene expression results are represented graphically as the mean ± standard error (SE) of the biological replicates. Data were analysed using the Mann-Whitney U test. For the LPS-induced lung injury, unpaired Student's t-test was used for comparison between the sham and vehicle control groups. One-way ANOVA followed by Dunnett's test were applied for comparison between treated groups and vehicle control groups. For the SARS-CoV-2-infected mouse model, virus burden and cytokine determination, data were analyzed by two-way ANOVA and Dunnet's multiple comparison to compare the means from each experimental group against vehicle group mean. For the analysis of histopathological scores, unpaired *t*-test was used to assess differences between experimental groups. All graphs were generated using GraphPad Prism 7 software. Statistical differences are displayed as * $p < 0.05$; ** $p < 0.01$; *** $p < 0.001$; **** $p < 0.0001$.

## 3. Results

AG5 compound was identified as a novel anti-inflammatory drug after a short screening of many andrographolide derivatives tested within an inflammatory scenario associated to viral infection in a transgenic zebrafish larvae model. Fig. 1 shows the compounds which showed significant activity, including the parent andrographolide.

3.1. Preliminary screening of andrographolide derivatives in transgenic zebrafish model

A significantly lower expression of the SVCV N gene was observed when the larvae were treated with AG1, AG4 and AG5, compared to the untreated control larvae (Fig. 2A). The larvae treated with AG3 did not show these differences in replication. The infection with SVCV produced an increase in the expression of IL-6 gen, and the AG4 and AG5 treatments also significantly decrease it (Fig. 2B). In the study of neutrophil
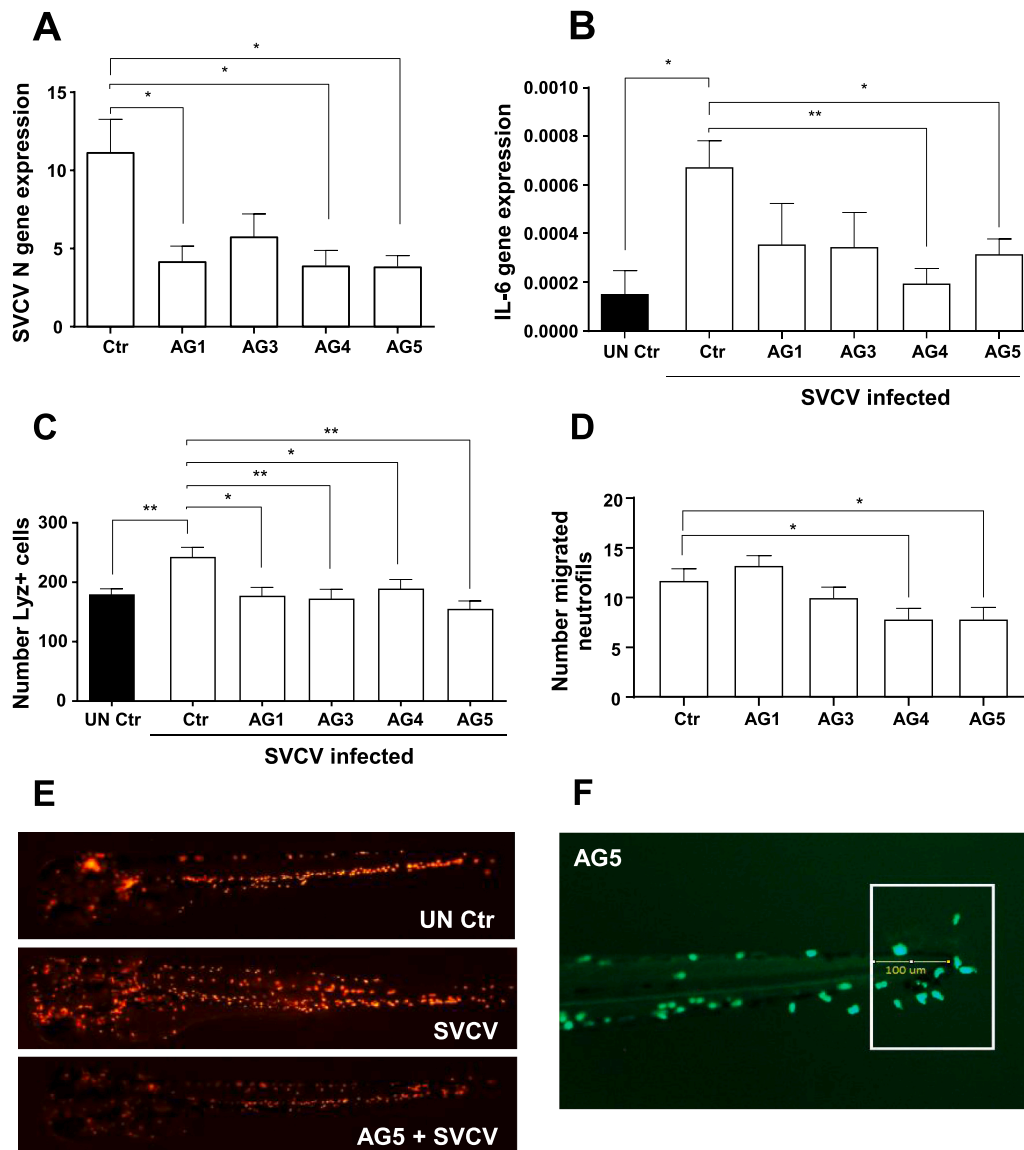
Fig. 2. Preliminary screening of andrographolide derivatives in transgenic zebrafish model. Bath concentration of andrographolide and derivatives was adjusted according to their water solubility pattern: AG1, AG3 5 μM; AG4, AG5 10 μM. A. SVCV N gene expression in larvae treated with AG1, AG3, AG4 or AG5 and infected with SVCV, compared to the untreated control (Ctr) ($n = 3$). B. IL-6 gene expression in larvae treated with AG1, AG3, AG4 or AG5 and infected with SVCV, compared to the untreated control (Ctr), or the uninfected and untreated control (UN Ctr) ($n = 3$). C. Total number of immune cells labelled (Lyz+ cells) in larvae (3 dpf) infected with SVCV and treated with AG1, AG3, AG4 or AG5, compared to the untreated control (Ctr), or the uninfected and untreated control (UN Ctr) ($n = 2$). D. Neutrophil migration to the regenerative tissues in the transgenic line Tg(*mpx*:GFP, 3 dpf) after cutting larvae tail with a razor and treatment with AG5 compared to the untreated group (Ctr) ($n = 2$). E. Images of whole larvae taken under the fluorescence microscope. **F**. Image of neutrophil migration to the regenerative tissues 24 h after challenge. Data are means ± SD.* $p < 0.05$; ** $p < 0.01$.

migration under SVCV infection an increase in the total number of Lyz+ cells was observed when the larvae were infected with SVCV. However, the treatment with the different andrographolide derivatives was able to decrease this number during the viral infection (Fig. 2C). Moreover, When we analyzed the inflammatory effect caused by a wound in the tail of the larvae and the number of neutrophils that come to the wound site were counted using the transgenic line Tg(*mpx*:GFP), only AG4 and AG5 treatments were capable of successfully decrease this inflammatory stimulus after 24 h, when the resolution of the inflammatory response is desirable to avoid detrimental effects for the organism (Fig. 2D-F).

3.2. AG5 inhibits caspase-1 and modulates innate immune responses in vitro

AG5 acted over the inflammasome by reducing caspase-1 activity. Since caspase-1 activity leads to processing and releasing of relevant pro-inflammatory cytokines such as IL-1β, we wanted to check how the AG5 treatment interfered with this process. To this end, human monocites THP-1 cell line was treated with AG5 and subjected them to different inflammatory stimuli, such as bacterial lipopolysaccharide (LPS) in combination with adenosine triphosphate (ATP), a second stimulus that promotes inflammasome activation. The specific inhibitor of the caspase-1, Ac- YVAD-CHO, was also included for detection of caspase-1 activation. As a positive control, treatment with andrographolide was also carried out over activated cells. As expected, stimulation with LPS increased caspase-1 activity, and treatment with

andrographolide was able to decrease this activity, but not AG5. However, when a major inflammatory stimulus was tested, combining LPS in a first stimulus and a second stimulus with ATP, THP-1 cells exhibited a much higher caspase-1 activity. Under these conditions, AG5 treatment significantly decreased such caspase-1 activity (Fig. 3A). The amount of cytokine IL-1β protein produced under such stimuli was also quantified. LPS stimulus alone did not increase IL-1β secretion, however, when the double LPS-ATP stimulus was used, a higher amount of IL-1β was observed, which was significantly reduced by AG5 treatment (Fig. 3B).

In an effort to better understanding AG5 mechanism of action in cells from the immune system, primary dendritic cells (DC) responses were studied in AG5 presence. For the purpose of comparison, dexamethasone was included in same conditions as a representative steroid with marked immunosuppression activity [26]. DC are the major professional antigen presenting cells, serving as a hub for initiating and shaping the nature of the immune responses through cytokine secretion together with processing and presentation of antigens to specific T-cells [27]. Secretion of cytokines defined not only DC activation status but also the signals delivered to other cells in the immune system triggering adaptive immune responses [28,29]. When moDC were stimulated via toll-like receptor 4 (TLR4) with LPS, used as a surrogate for bacterial infections [30], AG5 was able to significantly reduce IL-10 and IL-12, but to lower extent than dexamethasone (Fig. 3C-D). No alterations due to AG5 were observed in IL-1β, IL-6 or TNFα secretion, whereas dexamethasone strongly reduced IL-1β levels (Fig. 3E-G). On the other hand, when toll-like receptor 3 (TLR3) activation with polyinosinic:polycytidylic acid (Poly I:C) was used for mimicking viral infections and inducing antiviral immune responses [30], AG5 only reduced IL-1β levels, whereas dexamethasone significantly diminished all cytokines tested. Noteworthy, when no other stimuli were present, AG5 significantly reduced IL-12 and IL-6 and in the latter case to similar levels than dexamethasone (Fig. 3D and F). These results indicated that AG5 immunomodulation not only showed a different pattern of secretion on moDC than dexamethasone, but also different pattern of cytokine inhibition.

3.3. AG5 minimizes inflammatory response in a mouse model of LPS-induced lung injury

Given the particular AG5 immunomodulatory properties shown in in vitro systems, its activity was tested in experimental mice models. AG5 was evaluated for its possible inhibitory effects on LPS-induced pulmonary neutrophilia in male BALB/c mice. AG5 (30 mg/kg) was administered intravenously immediately after the LPS intratracheal instillation, and mice received AG5 continued dosing once per day for 3 more days. Animals were euthanized 4 h after the last administration, and bronchoalveolar lavage fluid (BALF) and serum samples were harvested for IL-1β, IL-6, and TNFα level determination. Moreover, lung tissue samples were collected for histopathological evaluation by hematoxylin and eosin (H&E) staining. Similar to previous in vitro experiments, dexamethasone (5 mg/kg) was used as positive control for anti-inflammatory therapy (Fig. 4A).

Following LPS instillation, levels of pro-inflammatory cytokines IL-1β and IL-6 and TNFα elevated sharply in BALF and serum. These effects were attenuated by AG5 or dexamethasone, reducing significantly levels of IL-1β in BALF or IL-1β and IL-6 in serum (Fig. 4B-E). However, whereas dexamethasone eliminates TNFα from serum, no effect was observed under AG5 treatment. This apparent discrepancy supported the rationale of a distinctive immunomodulation activity of AG5, without a full suppression of the primary immune response.

LPS challenge involved significant histopathological alteration in lung tissue with multifocal to diffuse inflammatory cell infiltration as major lesions, indicating the successful induction of lung inflammation (Fig. 4F). Severity of lung injury was markedly reduced with AG5 or dexamethasone as compared to the vehicle-treated group. They both also limited the extension of inflammatory cell infiltration.

Histopathological scores also showed that AG5 (2.2/5) and dexamethasone (1.6/5) significantly alleviated lung tissue damage as compared with their control vehicle-treated mice counterparts (2.8/5) (Fig. 4G) [23]. Remarkably, AG5 action was not as dramatic as dexamethasone.

3.4. AG5 exhibits in vivo anti-inflammatory efficacy in the SARS-CoV-2-infected mouse model

On the basis of the above mentioned anti-inflammatory activity, and under the health emergency created by the COVID-19 pandemic, we aimed at elucidating the in vivo efficacy of AG5 in an established animal model of SARS-CoV-2 infection, K18-hACE2 mouse [24,31]. After viral challenge, mice were treated with vehicle, AG5 or AG5 + remdesivir (Fig. 5A). Viral burden in the lungs was quantified by RT-qPCR for each experimental group (Fig. 5B). A reduction of about 1 log unit in lungs of SARS-CoV-2 viral load in the lungs was found in AG5-treated mice as compared with vehicle-treated animals. No additive effect was found when AG5 was combined with remdesivir. However, remdesivir-treated mice exhibited a reduction of 1.5 log units relative to vehicle-treated animals.

Lower levels of mRNA expression of pro-inflammatory cytokines (IL-1β and IL-6) were detected in the lungs of SARS-CoV-2 infected mice treated with AG5 or with AG5 + remdesivir (Fig. 5C-D) as compared with vehicle-treated group. Conversely, such reduction was not observed in animals treated only with remdesivir, supporting the specific cytokine inhibition by AG5. Histopathological evaluation of lung sections (Fig. 5E) confirmed that SARS-CoV-2-challenged vehicle-treated mice displayed moderate to severe inflammatory lesions, which were strongly minimized in all treated groups. Analysis of histopathological scores indicated a significant decrease of lung inflammation in AG5-treated mice and AG5 + remdesivir-treated mice over mice receiving vehicle only (Fig. 5F). Furthermore, remdesivir alone reduced lung inflammation as a secondary effect of SARS-CoV-2 inhibition of replication, as already shown for other antivirals [32]. In addition, AG5-treated group showed a reduction in the percentage of lung area with lesions as compared with their control (vehicle) (Fig. 5G). Remarkably, some AG5-treated mice showed the lowest inflammatory scores and the lowest percentages of lung area with lesions. All in all, these experiments showed that AG5 combines antiviral and anti-inflammatory activity against SARS-CoV-2 infection, besides being able to modulate the innate immune response.

3.5. AG5 shows good toxicological profile

AG5 toxicological preclinical profile under good laboratory practices (GLP) was evaluated according to ICH guideline M3 (R2) over one rodent animal model (rat, Wistar), and a non-rodent mammal model (rabbit, New Zealand White). According to 7-day dose research finding (DRF) studies, the maximum tolerated dose (MTD) was stablished at 30 mg/kg for mouse and rat, and 15 mg/kg for rabbit. No lethality in any of the animals was observed at these dose ranges, and no alterations were detected in the clinical examinations [33]. No change in hematological or biochemical parameters was observed in any of the animals. In any case, the post-mortem pathological evaluation of tissue samples (kidneys, spleen, heart, liver, thymus and ovaries/testes) from all the animals did not show any damage. Finally, no weight loss was reported in any of the animals. All data corresponding to these studies are presented in the Supporting Information (Tables S1-S12).

Animal models were validated by determination of the intrinsic clearance assay over cryopreserved hepatocytes of human, rat and rabbit [34]. No relevant differences were found in the hepatic metabolism of AG5, the result obtained of intrinsic clearance at 120 min was 96.4 for human, 81.9 for rat and 85.3 for rabbit, which results in a CL_{int} of 1.2, 1.7 and 1.7, in human, rat and rabbit, respectively (Table S13).
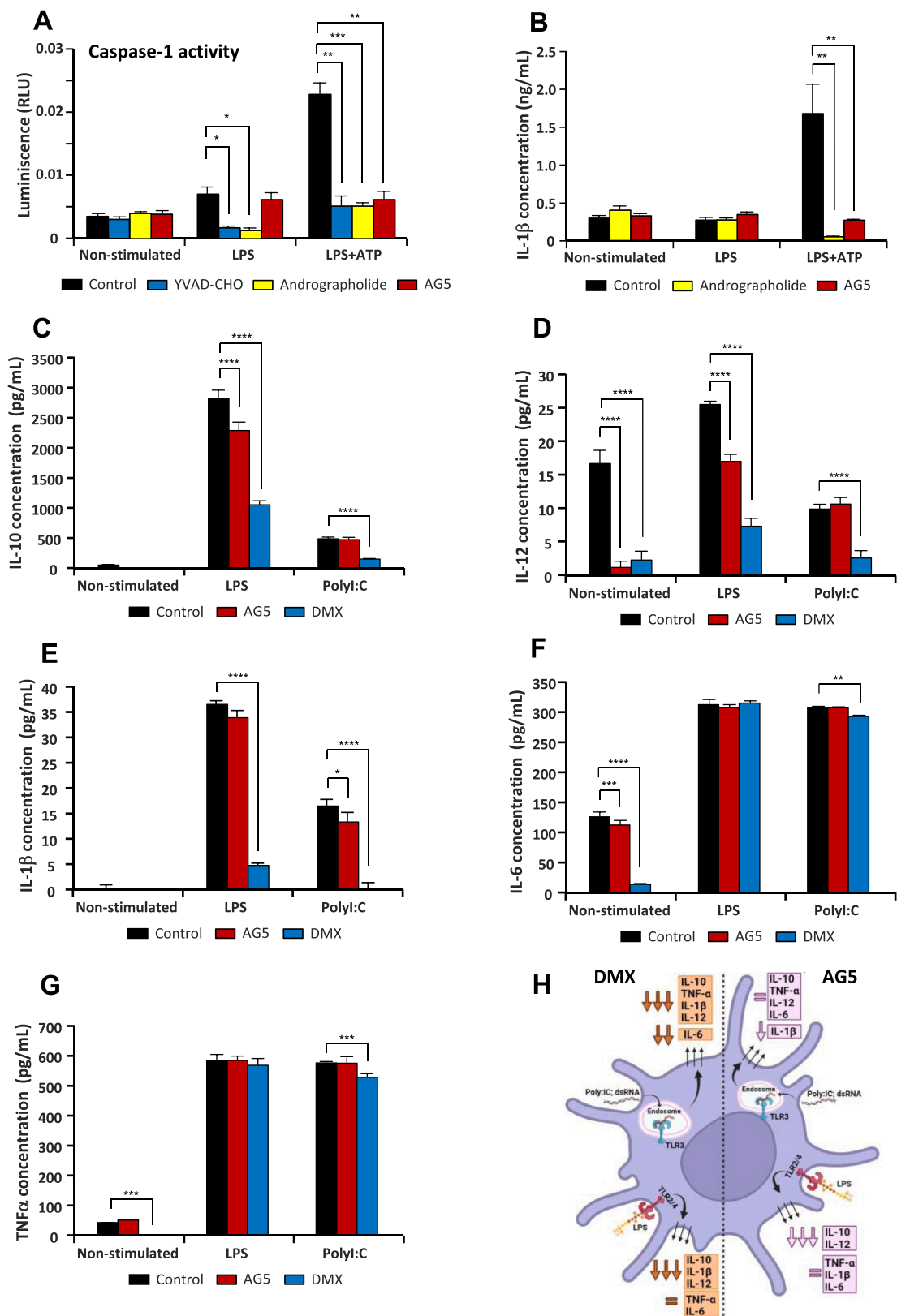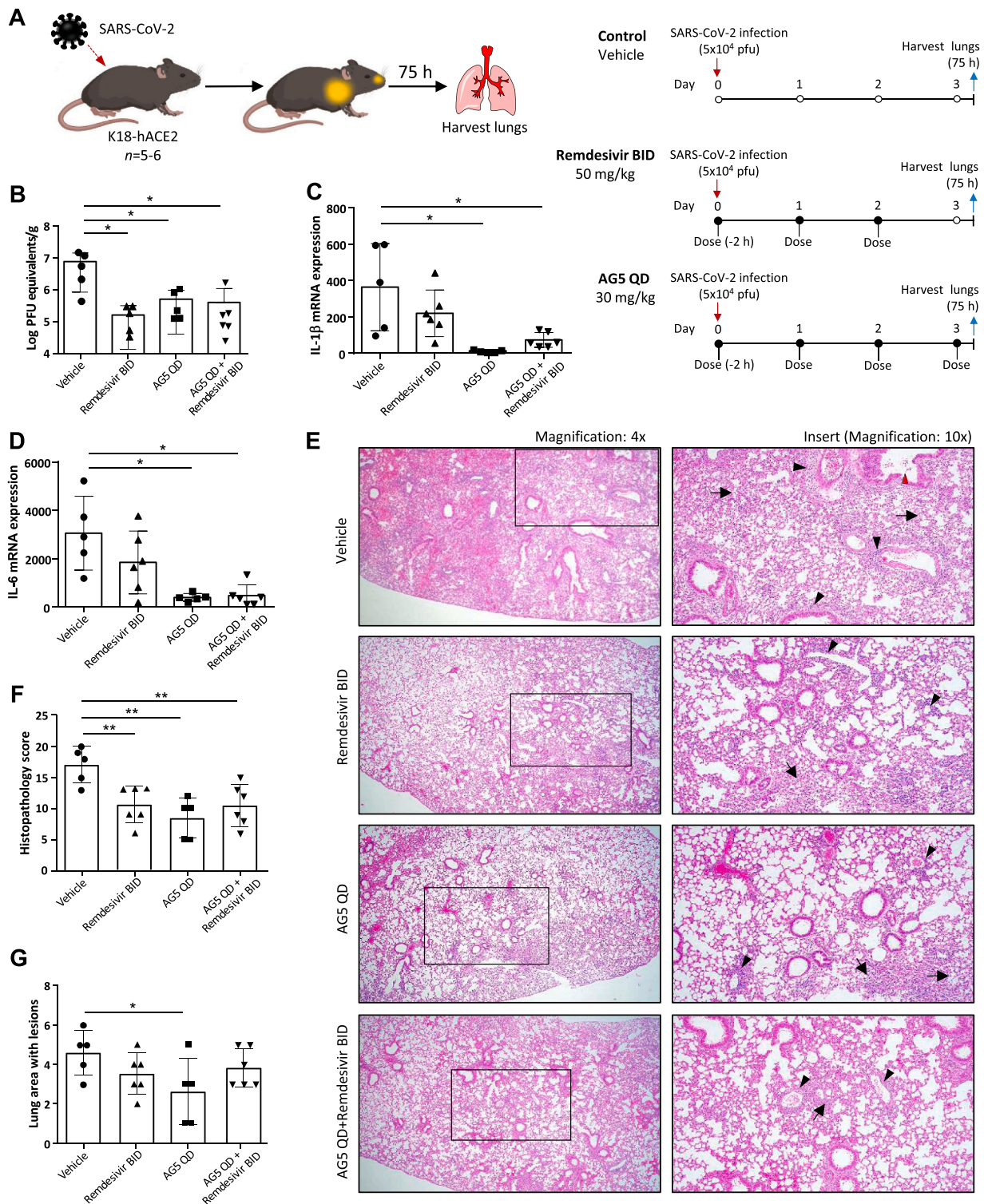
Fig. 3. AG5 inhibits caspase-1 in THP-1 cells and modulates immune response in DC cells. A. Under a major inflammatory stimulus, by combining a first stimulus with LPS and a second stimulus with ATP, THP-1 cells presented a much higher caspase-1 activity, and in these conditions andrographolide or AG5 decreased significantly this excessive caspase-1 activity. **B.** Under the double LPS-ATP stimulus, a higher amount of IL-1β was observed in THP-1 cells, and this quantity was significantly decreased with andrographolide or AG5. **C** to **G.** moDC patterns of cytokine secretion in non-stimulated cells, or upon TLR 3 signaling (PolyI:C) or TLR4 stimulation (LPS), in presence or absence of AG5 or dexamethasone (DXM): (C) IL-10; (D) IL-12; (E) IL-1β; (F) IL-6; (G) TNFα. **F.** Artistic representation (BioRender) of a moDC showing differences in cytokine release of LPS or Poly:IC-stimulation after DXM or AG-5 treatment. Data are means ± SD ($n = 3$). * $p < 0.05$; * * $p < 0.01$; *** $p < 0.001$; **** $p < 0.0001$.
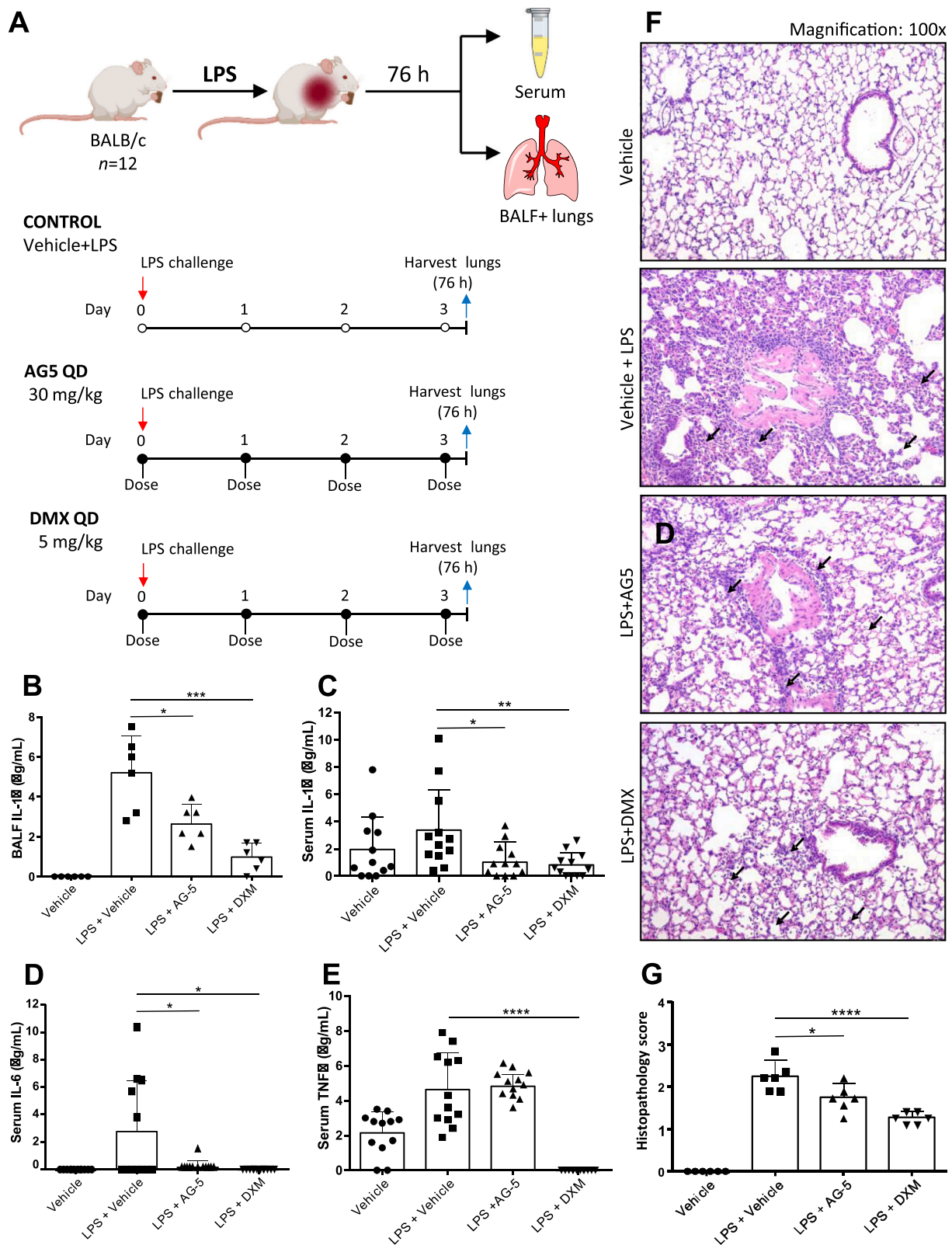
Fig. 4. AG5 minimizes inflammatory response in a mouse model of LPS-induced lung injury. A. Schematic of LPS challenge of BALB/c mice model and sample collection after end-point. Mice ($n = 12$) were sensitized by intratracheal instillation with 2 μg LPS in 20 μL phosphate buffer saline (PBS) per mouse and intra-venously treated with either 30 mg/kg AG5 or 5 mg/kg dexamethasone (DMX) once daily for 3 days. Animal were humanly euthanized 4 h after the last dose. B to E. Cytokine secretion patterns obtained from BALF and serum samples from 6 animals in every group (mice #1–6), as determined by ELISA. F. Lungs were harvested from the other six animals in each group (mice #7–12), formalin fixed, paraffin-embedded and 5 μm sections stained for hematoxylin and eosin. Regions where inflammation was detected are indicated by arrows. **G.** Semi-quantitative lesion score of the pulmonary inflammation according to [24]. * $p < 0.05$; ** $p < 0.01$; *** $p < 0.001$; **** $p < 0.0001$.

Fig. 5. AG5 exhibits in vivo anti-inflammatory efficacy in the SARS-CoV-2-infected mouse model. A. Schematic of the K18-hACE2 model of SARS-CoV-2 infection and sample collection after end-point. Mice ($n = 5$–6) were intranasally infected with 5×10^4 pfu of SARS-CoV-2 and intravenously treated with 30 mg/kg AG5 once daily (QD) for 3 days or 50 mg/kg remdesivir twice daily (BID) for 2 days. In addition, one mice group received both AG5 (30 mg/kg QD) and remdesivir (50 mg/kg BID). Animal were humanly euthanized 3 h after the last dose. B. SARS-CoV-2 viral burden in the lungs. Virus load was quantified in the right lung homogenate of every mouse. C, D. Cytokine secretion patterns obtained from the right lung homogenate of every mouse, as determined by RT-qPCR: (D) IL-1β; (E) IL-6. E. Representative lung histopathological sections. Left lung from every mouse in all groups was harvested, formalin fixed, paraffin-embedded and 5 μm sections stained for hematoxylin and eosin. Left panel: magnification 4x; right panel (insert): magnification 10x. Lung areas where inflammation was assessed are highlighted by black boxes, with the corresponding magnification image at the right. Arrows indicate diffuse mononuclear cell infiltrates in the alveolar spaces, black arrowheads mark large multifocal perivascular and peribronchiolar mononuclear infiltrates, and red arrowheads show bronchioles with detached epithelium and inflammatory cells in the lumen. F. Semi-quantitative lesion score of the pulmonary inflammation according to [23]. G. Percentage of lung area with lesions examined in left lung samples. * $p < 0.05$; ** $p < 0.01$.

4. Discussion

The outbreak of SARS-CoV-2 pandemic inspired many research and clinical teams to screen clinically approved anti-inflammatory drugs, as dexamethasone, in an attempt to reduce the mortality rate among COVID-19 patients with severe respiratory and systemic issues [2]. However, adverse effects of glucocorticoids on innate immunity, especially in COVID-19 outpatients, was prominent [4]. A study on SARS-CoV-2 infected golden Syrian hamster used as preclinical model and treated with a combination of methylprednisolone and remdesivir, confirmed that such anti-inflammatory activity of steroids is overshadowed by its anti-clearance effect at the early stage of infection [35]. Conversely, from the very beginning, our strategy was to obtain an immunomodulatory drug able to inhibit the cytokine storm with moderate influence over the primary immune response.

In this sense, a preliminary study of different andrographolide (AG1) synthetic derivatives over zebrafish larvae infected with SVCV, showed that AG4 and AG5 compounds were the best candidates to successfully decrease the inflammatory stimulus. Moreover, as AG5 is a known metabolite of AG1 with high absorption rate at the duodenum and jejunum [14], we chose this molecule for the further therapeutic and toxicology study.

The TLR4 signaling pathway initiated by LPS triggered immune response, emulating infection of cells by microorganism, involves induction of NF-κβ family of transcription factors and, subsequently, activation of inflammation-related genes encoding pro- and anti-inflammatory cytokines. NF-κβ regulates expression of a wide spectrum of genes critically associated to inflammation and innate immunity [30,36]. Here, caspase-1 has a key role in NF-κβ activation and TNFα production in response to TLR4 stimulation [37,38]. We have shown AG5 performance as strong caspase-1 inhibitor under a major inflammatory stimulus and, therefore, it is plausible to think that AG5 mode of action went through selectively targeting NF-κβ transcriptional activity to reduce cytokine secretion. These results were also consistent with the mechanism of inflammation attenuation described for natural andrographolide, which inhibits NF-κβ activation through covalent modification of reduced cysteine 62 of p50 [39].

The fact that AG5 differentially modulates immune activity in DC, instead of a radical immunosuppression, providing better therapeutic perspective that any glucocorticoid treatment, which administration timing impacts dramatically the overall response rate, not only in viral infections, but also in cancer immunotherapy [26,40]. Among the cytokines secreted by moDC, TNFα, IL-1β and IL-6 are considered pro-inflammatory cytokines whereas IL-10 is considered anti-inflammatory cytokine [41]. Conversely, IL-12 p70 is considered an important link between innate resistance and adaptive immunity. Among IL-12 functions are included regulation of T-cells and natural killers (NK) responses by favouring T_H1 differentiation and IFNγ induction [42]. Importantly, AG5 reduced IL-12 secretion but to lower extent than dexamethasone. In addition, the fact that AG5 reduced IL-10 secretion upon TLR4 stimulation and IL-1β upon TLR3.

stimulation suggested an immunoregulation pathway different from dexamethasone that remains to be explored. Consequently, any alteration on cytokine secretion by DC will have an impact on subsequent adaptive immune responses so it is plausible to think that effector lymphocytes will be affected by AG5-induced pattern of cytokines secretion by DC.

Antiviral efficacy of AG5 against SARS-CoV-2 is related with the primal compound andrographolide, which has shown to inhibit SARS-CoV-2 replication over Calu-3 cells in a dose-dependent manner [43]. Furthermore, computational studies showed that andrographolide covalently links to the main protease (M^{pro}) of SARS-CoV-2 [44,45], encoded by the *nsp5* gene and involved in production of functional polyproteins for maturation in host cells [46], which reduces virus replication. This mechanism has also been proved recently for antiviral drug S-217622, currently in a phase 3 clinical trial [47]. AG5 was less

efficient as antiviral than inhibitors of RNA-dependent RNA polymerase (RdRp) already approved for clinical use in COVID-19 therapy, as remdesivir [48] and molnupiravir [49], however, its antiviral activity is complemented by favouring the immune response against the infection.

Toxicity studies under GLP conditions, confirmed 30 mg/kg dose in mouse and rat, and 15 mg/kg in rabbit as the maximum dose to be tested in preclinical testing (MTD) without discovering any toxicological alert to monitor. Validation of the animal models by determination of the intrinsic clearance in cryopreserved hepatocytes was informative in establishing safety margins and guiding selection of first in human (FIH) dose and human efficacious dose [50].

AG5 also presents additional advantages over the parent andrographolide, such as lower hepatic degradation and quick renal elimination, which provides a satisfactory toxicological profile [15,51]. Intrinsic clearance (CL_{int}) in human cryopreserved hepatocytes of AG5 is 1.2 μL/min/mg, whereas the reported value for andrographolide in human liver microsomes is 6.2 μL/min/mg [52]. In addition, AG5 solubility is almost 2 orders higher than andrographolide [53], which notably improves bioavailability. Taken together the anti-inflammatory and antiviral performance shown here by AG5 together with its preclinical tolerability, proves that AG5 has potential for translation into clinical trials in treatment of cytokine storm associated to infectious diseases, being COVID-19 the most immediate example. The selected patient niche must be outpatients with bilateral pneumonia caused by SARS-CoV-2, who receive AG5 alone or in combination with an antiviral (e.g., remdesivir), should the phase I trial over healthy adults prove the concomitant administration of both drugs is safe.

Beyond COVID-19, many potential applications of great interest are opened for AG5. For example, novel immunotherapeutic strategies including CAR-T cells and bispecific T cell engagers, redirect T cells toward tumor cells, facilitating the formation of a cytotoxic synapse and resulting in subsequent tumor cell killing, which triggers a release of pro-inflammatory cytokines, generating a Cytokine Release Syndrome (CRS) [54]. The incidence of CRS is around 80–90% in patients with hematological malignancies treated with these novel T-cell therapies, but it is usually well controlled with tocilizumab, an IL-6 antagonist that can precisely block interleukin-6 (IL-6). If this therapy fails to control CRS, corticosteroids are the second step. In fact, novel strategies directed to mitigate CRS are considering the possibility of the prophylactic use of tocilizumab. Since AG5 is a potent inhibitor non-steroidal anti-inflammatory and selective immune regulator (with a marked IL-6 inhibitory effect) that preserves innate immunity, it could be a very attractive drug, due to its excellent safety profile, for investigation on CRS prophylaxis programs.

CRediT authorship contribution statement

Pablo Botella-Asunción: Conceptualization, Methodology, Visualization, Funding acquisition, Project administration, Supervision, Writing – original draft, Writing – review & editing. **Eva M. Rivero-Buceta:** Investigation, Validation, Formal analysis. **Carla Vidaurre-Agut:** Investigation, Validation. **Raquel Lama:** Investigation, Validation, Formal analysis. **Magalí Rey-Campos:** Investigation, Validation. **Alejandro Moreno:** Investigation, Validation. Laura Mendoza: Investigation, Validation, Formal analysis,Visualization. **Patricia Mingo-Casas:** Investigation, Validation, Formal analysis. **Estela Escribano-Romero:** Investigation, Validation. **Alfonso Gutierrez-Adan:** Investigation, Validation. **Juan Carlos Saiz:** Supervision. Cristian Smerdou: Investigation, Validation, Formal analysis. **Gloria Gonzalez:** Investigation, Validation, Formal analysis. **Felipe Prosper:** Methodology, Writing – review & editing. **Josepmaría Argemi:** Methodology, Writing – review & editing. **Jesus San Miguel:** Funding acquisition, Writing – review & editing. **Pedro J. Sanchez-Cordón:** Methodology, Investigation, Validation, Formal analysis, Writing – original draft, Writing – review & editing. **Antonio Figueras:** Methodology, Supervision, Writing – original draft, Writing – review & editing. Jose Manuel

Quesada-Gomez: Writing – original draft, Writing – review & editing. **Beatriz Novoa:** Methodology, Formal analysis, Visualization, Supervision, Writing – original draft, Writing – review & editing. **María Montoya:** Methodology, Visualization, Funding acquisition, Supervision, Writing – original draft, Writing – review & editing. **Miguel A. Martín-Acebes:** Methodology, Visualization, Funding acquisition, Supervision, Writing – original draft, Writing – review & editing. **Antonio Pineda-Lucena:** Methodology, Visualization, Supervision, Writing – original draft, Writing – review & editing. **Jose María Benlloch:** Conceptualization, Methodology, Funding acquisition, Project administration, Supervision, Writing – original draft, Writing – review & editing.

Declaration of Competing Interest

The authors declare the following financial interests/personal relationships which may be considered as potential competing interests: "AG5 andrographolide derivative for use in the treatment of inflammatory diseases associated with a cytokine storm" is a formal Spanish Patent (ES2908500) since March 15th, 2023. PBA, ERB, CVA, BN, AF, CS, GGA, FP, JA, APL and JMB are co-inventors of this patent.

Data Availability

Data will be made available on request.

Acknowledgments

Supplementary Materials

Materials and Methods.
Synthesis and characterization of andrographolide synthetic derivatives.
AG5 in vivo toxicological profile.
Additional references.

Appendix A. Supporting information

Supplementary data associated with this article can be found in the online version at doi:10.1016/j.biopha.2023.115882.

References

[1] D. Blanco-Melo, B.E. Nilsson-Payant, W. Liu, J.K. Lim, R.A. Albrecht, R. Benjamin, D. Blanco-melo, B.E. Nilsson-payant, W. Liu, S. Uhl, D. Hoagland, Article imbalanced host response to SARS-CoV-2 drives development of COVID-19 ll ll article imbalanced host response to SARS-CoV-2 drives development of COVID-19, e9, Cell 181 (2020) 1036–1045, https://doi.org/10.1016/j.cell.2020.04.026.

[2] The RECOVERY Collaborative Group, Dexamethasone in hospitalized patients with Covid-19, N. Engl. J. Med. 384 (2021) 693–704, https://doi.org/10.1056/nejmoa2021436.

[3] J. Liu, S. Zhang, X. Dong, Z. Li, Q. Xu, H. Feng, J. Cai, S. Huang, J. Guo, L. Zhang, Y. Chen, W. Zhu, H. Du, Y. Liu, T. Wang, L. Chen, Z. Wen, D. Annane, J. Qu, D. Chen, Corticosteroid treatment in severe COVID-19 patients with acute respiratory distress syndrome, J. Clin. Invest. 130 (2020) 6417–6428, https://doi.org/10.1172/JCI140617.

[4] A.K. Sahu, R. Mathew, R. Bhat, C. Malhotra, J. Nayer, P. Aggarwal, S. Galwankar, Steroids use in non-oxygen requiring COVID-19 patients: a systematic review and meta-Analysis, Qjm 114 (2021) 455–463, https://doi.org/10.1093/qjmed/hcab212.

[5] N. Lee, K.C. Allen Chan, D.S. Hui, E.K.O. Ng, A. Wu, R.W.K. Chiu, V.W.S. Wong, P. K.S. Chan, K.T. Wong, E. Wong, C.S. Cockram, J.S. Tam, J.J.Y. Sung, Y.M.D. Lo, Effects of early corticosteroid treatment on plasma SARS-associated Coronavirus RNA concentrations in adult patients, J. Clin. Virol. 31 (2004) 304–309, https://doi.org/10.1016/j.jcv.2004.07.006.

[6] B. Cao, H. Gao, B. Zhou, X. Deng, C. Hu, C. Deng, H. Lu, Y. Li, J. Gan, J. Liu, H. Li, Y. Zhang, Y. Yang, Q. Fang, Y. Shen, Q. Gu, X. Zhou, W. Zhao, Z. Pu, L. Chen, B. Sun, X. Liu, C.D. Hamilton, L. Li, Adjuvant corticosteroid treatment in adults with influenza A (H7N9) viral pneumonia, Crit. Care Med. 44 (2016) e318–e328, https://doi.org/10.1097/CCM.0000000000001616.

[7] Y.M. Arabi, Y. Mandourah, F. Al-Hameed, A.A. Sindi, G.A. Almekhlafi, M. A. Hussein, J. Jose, R. Pinto, A. Al-Omari, A. Kharaba, A. Almotairi, K. Al Khatib, B. Alraddadi, S. Shalhoub, A. Abdulmomen, I. Qushmaq, A. Mady, O. Mady, A. M. Al-Aithan, R. Al-Raddadi, A. Ragab, H.H. Balkhy, A. Balkhy, A.M. Deeb, H. Al Mutairi, A. Al-Dawood, L. Merson, F.G. Hayden, R.A. Fowler, Corticosteroid therapy for critically ill patients with middle east respiratory syndrome, Am. J. Respir. Crit. Care Med. 197 (2018) 757–767, https://doi.org/10.1164/rccm.201706-1172OC.

[8] H. Ledford, Hundreds of COVID trials could provide a deluge of new drugs, Nature 603 (2022) 25–27, https://doi.org/10.1038/d41586-022-00562-0.

[9] A. Panossian, A. Hovhannisyan, G. Mamikonyan, H. Abrahamian, E. Hambardzumyan, E. Gabrielian, G. Goukasova, G. Wikman, H. Wagner, Pharmacokinetic and oral bioavailability of andrographolide from Andrographis paniculata fixed combination Kan Jang in rats and human, Phytomedicine 7 (2000) 351–364, https://doi.org/10.1016/S0944-7113(00)80054-9.

[10] Z. Bao, S. Guan, C. Cheng, S. Wu, S.H. Wong, D.Michael Kemeny, B.P. Leung, W.S. Fred Wong, A novel antiinflammatory role for andrographolide in asthma via inhibition of the nuclear factor-κb pathway, Am. J. Respir. Crit. Care Med. 179 (2009) 657–665, https://doi.org/10.1164/rccm.200809-1516OC.

[11] L. Cui, F. Qiu, X. Yao, Isolation and identification of seven glucuronide conjugates of andrographolide in human urine, Drug Metab. Dispos. 33 (2005) 555–562, https://doi.org/10.1124/dmd.104.001958.

[12] X. Tian, S. Liang, C. Wang, B. Wu, G. Ge, S. Deng, K. Liu, L. Yang, X. Ma, Regioselective glucuronidation of andrographolide and its major derivatives: metabolite identification, isozyme contribution, and species differences, AAPS J. 17 (2015) 156–166, https://doi.org/10.1208/s12248-014-9658-8.

[13] X. He, J. Li, H. Gao, F. Qiu, K. Hu, X. Cui, X. Yao, Identification of a rare sulfonic acid metabolite of andrographolide in rats, Drug Metab. Dispos. 31 (2003) 983–985, https://doi.org/10.1124/dmd.31.8.983.

[14] Z.L.L. Ye, T. Wang, L. Tang, W. Liu, Z. Yang, J. Zhou, Z. Zheng, Z. Cai, M. Hu, Poor oral bioavailability of a promising anticancer agent andrographolide is due to extensive metabolism and efflux by P-glycoprotein, J. Pharm. Sci. 100 (2011) 5007–5017, https://doi.org/10.1002/jps.22693.

[15] C.A. Strott, Sulfonation and molecular action, Endocr. Rev. 23 (2002) 703–732, https://doi.org/10.1210/er.2001-0040.

[16] S. Peng, N. Hang, W. Liu, W. Guo, C. Jiang, X. Yang, Q. Xu, Y. Sun, Andrographolide sulfonate ameliorates lipopolysaccharide-induced acute lung injury in mice by down-regulating MAPK and NF-κB pathways, Acta Pharm. Sin. B. 6 (2016) 205–211, https://doi.org/10.1016/j.apsb.2016.02.002.

[17] W. Chanput, J.J. Mes, H.J. Wichers, THP-1 cell line: An in vitro cell model for immune modulation approach, Int. Immunopharmacol. 23 (2014) 37–45, https://doi.org/10.1016/j.intimp.2014.08.002.

[18] M.S.Miguel Rodrıguez-Pulido, Eva Calvo-Pinilla, Miryam Polo, Juan-Carlos Saiz, Raul Fernandez-Gonzalez, Eva Pericuesta, Alfonso Gutierrez-Adan, Francisco Sobrino, Miguel A. Martin-Acebes, Margarita Saez, Non-coding RNAs derived from the foot-and-mouth disease virus genome trigger broad antiviral activity against coronaviruses, Front. Immunol. 14 (2023) 1–12, https://doi.org/10.3389/fimmu.2023.1166725.

[19] J.M. Casasnovas, Y. Margolles, M.A. Noriega, M. Guzmán, R. Arranz, R. Melero, M. Casanova, J.A. Corbera, N. Jiménez-de-Oya, P. Gastaminza, U. Garaigorta, J. C. Saiz, M.Á. Martín-Acebes, L.Á. Fernández, Nanobodies protecting from lethal SARS-CoV-2 infection target receptor binding epitopes preserved in virus variants other than omicron, Front. Immunol. 13 (2022) 1–18, https://doi.org/10.3389/fimmu.2022.863831.

[20] T.P. Sheahan, A.C. Sims, R.L. Graham, V.D. Menachery, L.E. Gralinski, J.B. Case, S. R. Leist, K. Pyrc, J.Y. Feng, I. Trantcheva, R. Bannister, Y. Park, D. Babusis, M. O. Clarke, R.L. MacKman, J.E. Spahn, C.A. Palmiotti, D. Siegel, A.S. Ray, T. Cihlar,

R. Jordan, M.R. Denison, R.S. Baric, Broad-spectrum antiviral GS-5734 inhibits both epidemic and zoonotic coronaviruses, Sci. Transl. Med. 9 (2017) 9–11, https://doi.org/10.1126/scitranslmed.aal3653.

[21] C.D. Spinner, R.L. Gottlieb, G.J. Criner, J.R. Arribas López, A.M. Cattelan, A. Soriano Viladomiu, O. Ogbuagu, P. Malhotra, K.M. Mullane, A. Castagna, L.Y. A. Chai, M. Roestenberg, O.T.Y. Tsang, E. Bernasconi, P. Le Turnier, S.C. Chang, D. Sengupta, R.H. Hyland, A.O. Osinusi, H. Cao, C. Blair, H. Wang, A. Gaggar, D. M. Brainard, M.J. McPhail, S. Bhagani, M.Y. Ahn, A.J. Sanyal, G. Huhn, F. M. Marty, Effect of remdesivir vs standard care on clinical status at 11 days in patients with moderate COVID-19: a randomized clinical trial, JAMA - J. Am. Med. Assoc. 324 (2020) 1048–1057, https://doi.org/10.1001/jama.2020.16349.

[22] Y. Wang, D. Zhang, G. Du, R. Du, J. Zhao, Y. Jin, S. Fu, L. Gao, Z. Cheng, Q. Lu, Y. Hu, G. Luo, K. Wang, Y. Lu, H. Li, S. Wang, S. Ruan, C. Yang, C. Mei, Y. Wang, D. Ding, F. Wu, X. Tang, S. Ye, Y. Ye, B. Liu, J. Yang, W. Yin, A. Wang, G. Fan, F. Zhou, Z. Liu, X. Gu, J. Xu, L. Shang, Y. Zhang, L. Cao, T. Guo, Y. Wan, H. Qin, Y. Jiang, T. Jaki, F.G. Hayden, P.W. Horby, B. Cao, C. Wang, Remdesivir in adults with severe COVID-19: a randomised, double-blind, placebo-controlled, multicentre trial, Lancet 395 (2020) 1569–1578, https://doi.org/10.1016/S0140-6736(20)31022-9.

[23] C. Shackelford, G. Long, J. Wolf, C. Okerberg, R. Herbert, Qualitative and quantitative analysis of nonneoplastic lesions in toxicology studies, Toxicol. Pathol. 30 (2002) 93–96, https://doi.org/10.1080/01926230252824761.

[24] S.H. Sun, Q. Chen, H.J. Gu, G. Yang, Y.X. Wang, X.Y. Huang, S.S. Liu, N.N. Zhang, X.F. Li, R. Xiong, Y. Guo, Y.Q. Deng, W.J. Huang, Q. Liu, Q.M. Liu, Y.L. Shen, Y. Zhou, X. Yang, T.Y. Zhao, C.F. Fan, Y. Sen Zhou, C.F. Qin, Y.C. Wang, A mouse model of SARS-CoV-2 infection and pathogenesis, Cell Host Microbe 28 (2020) 124–133.e4, https://doi.org/10.1016/j.chom.2020.05.020.

[25] S.R. Black, J.W. Nichols, K.A. Fay, S.R. Matten, S.G. Lynn, Evaluation and comparison of in vitro intrinsic clearance rates measured using cryopreserved hepatocytes from humans, rats, and rainbow trout, Toxicology 457 (2021), 152819, https://doi.org/10.1016/j.tox.2021.152819.

[26] A.J. Giles, M.K.N.D. Hutchinson, H.M. Sonnemann, J. Jung, P.E. Fecci, N. M. Ratnam, W. Zhang, H. Song, R. Bailey, D. Davis, C.M. Reid, D.M. Park, M. R. Gilbert, Dexamethasone-induced immunosuppression: Mechanisms and implications for immunotherapy, J. Immunother. Cancer 6 (2018) 1–13, https://doi.org/10.1186/s40425-018-0371-5.

[27] L. Marongiu, M. Valache, F.A. Facchini, F. Granucci, How dendritic cells sense and respond to viral infections, Clin. Sci. 135 (2021) 2217–2242, https://doi.org/10.1042/CS20210577.

[28] R.A. Backer, H.C. Probst, B.E. Clausen, Classical DC2 subsets and monocyte-derived DC: delineating the developmental and functional relationship, Eur. J. Immunol. (2023), 2149548, https://doi.org/10.1002/eji.202149548.

[29] R.G. Spallanzani, N.I. Torres, D.E. Avila, A. Ziblat, X.L.R. Iraolagoitia, L.E. Rossi, C. I. Domaica, M.B. Fuertes, G.A. Rabinovich, N.W. Zwirner, Regulatory dendritic cells restrain NK Cell IFN-γ production through mechanisms involving NKp46, IL-10, and MHC Class I–specific inhibitory receptors, J. Immunol. 195 (2015) 2141–2148, https://doi.org/10.4049/jimmunol.1403161.

[30] T. Kawai, S. Akira, The role of pattern-recognition receptors in innate immunity: update on Toll-like receptors, Nat. Immunol. 11 (2010) 373–384, https://doi.org/10.1038/ni.1863.

[31] E.S. Winkler, A.L. Bailey, N.M. Kafai, S. Nair, B.T. McCune, J. Yu, J.M. Fox, R. E. Chen, J.T. Earnest, S.P. Keeler, J.H. Ritter, L.I. Kang, S. Dort, A. Robichaud, R. Head, M.J. Holtzman, M.S. Diamond, SARS-CoV-2 infection of human ACE2-transgenic mice causes severe lung inflammation and impaired function, Nat. Immunol. 21 (2020) 1327–1335, https://doi.org/10.1038/s41590-020-0778-2.

[32] K.M. White, R. Rosales, S. Yildiz, T. Kehrer, L. Miorin, E. Moreno, S. Jangra, M. B. Uccellini, R. Rathnasinghe, L. Coughlan, C. Martinez-Romero, J. Batra, A. Rojc, M. Bouhaddou, J.M. Fabius, K. Obernier, M. Dejosez, M.J. Guillén, A. Losada, P. Avilés, M. Schotsaert, T. Zwaka, M. Vignuzzi, K.M. Shokat, N.J. Krogan, A. García-Sastre, Plitidepsin has potent preclinical efficacy against SARS-CoV-2 by targeting the host protein eEF1A, Science 371 (2021) 926–931, https://doi.org/10.1126/science.abf4058.

[33] S. Irwin, Comprehensive observational assessment: Ia. A systematic, quantitative procedure for assessing the behavioral and physiologic state of the mouse, Psychopharmacologia 13 (1968) 222–257, https://doi.org/10.1007/BF00401402.

[34] R.S. Obach, Prediction of human clearance of twenty-nine drugs from hepatic microsomal intrinsic clearance data: an examination of in vitro half-life approach and nonspecific binding to microsomes, Drug Metab. Dispos. 27 (1999) 1350–1359.

[35] Z. Ye, S. Yuan, J.F. Chan, A.J. Zhang, Y. Yu, C.P. Ong, D. Yang, C.C. Chan, K. Tang, J. Cao, V.K. Poon, C.C. Chan, J. Cai, H. Chu, K. Yuen, D. Jin, C. Yu, C.P. Ong, D. Yang, C.C. Chan, K. Tang, J. Cao, Beneficial effect of combinational methylprednisolone and remdesivir in hamster model of SARS-CoV-2 infection, Emerg. Microbes Infect. 10 (2021) 291–304, https://doi.org/10.1080/22221751.2021.1885998.

[36] R. Medzhitov, T. Horng, Transcriptional control of the inflammatory response, Nat. Rev. Immunol. 9 (2009) 692–703, https://doi.org/10.1038/nri2634.

[37] S.M. Miggin, E. Pålsson-McDermott, A. Dunne, C. Jefferies, E. Pinteaux, K. Banahan, C. Murphy, P. Moynagh, M. Yamamoto, S. Akira, N. Rothwell, D. Golenbock, K.A. Fitzgerald, L.A.J. O'Neill, NF-κB activation by the Toll-IL-1 receptor domain protein MyD88 adapter-like is regulated by caspase-1, Proc. Natl. Acad. Sci. U. S. A. 104 (2007) 3372–3377, https://doi.org/10.1073/pnas.0608100104.

[38] J. Staal, T. Bekaert, R. Beyaert, Regulation of NF-κB signaling by caspases and MALT1 paracaspase, Cell Res 21 (2011) 40–54, https://doi.org/10.1038/cr.2010.168.

[39] Y.-F. Xia, B.-Q. Ye, Y.-D. Li, J.-G. Wang, X.-J. He, X. Lin, X. Yao, D. Ma, A. Slungaard, R.P. Hebbel, N.S. Key, J.-G. Geng, Andrographolide attenuates inflammation by inhibition of NF-κB activation through covalent modification of reduced cysteine 62 of p50, J. Immunol. 173 (2004) 4207–4217, https://doi.org/10.4049/jimmunol.173.6.4207.

[40] J.S. Weber, F.S. Hodi, J.D. Wolchok, S.L. Topalian, D. Schadendorf, J. Larkin, M. Sznol, G.V. Long, H. Li, I.M. Waxman, J. Jiang, C. Robert, Safety profile of nivolumab monotherapy: a pooled analysis of patients with advanced melanoma, J. Clin. Oncol. 35 (2017) 785–792, https://doi.org/10.1200/JCO.2015.66.1389.

[41] H. Fouladseresht, A. Ghamar Talepoor, N. Eskandari, M. Norouzian, B. Ghezelbash, M.R. Beyranvand, S.A. Nejadghaderi, K. Carson-Chahhoud, A.A. Kolahi, S. Safiri, Potential immune indicators for predicting the prognosis of COVID-19 and trauma: similarities and disparities, Front. Immunol. 12 (2022) 1–22, https://doi.org/10.3389/fimmu.2021.785946.

[42] K. Hildenbrand, I. Aschenbrenner, F.C. Franke, O. Devergne, M.J. Feige, Biogenesis and engineering of interleukin 12 family cytokines, Trends Biochem. Sci. 47 (2022) 936–949, https://doi.org/10.1016/j.tibs.2022.05.005.

[43] K. Sa-Ngiamsuntorn, A. Suksatu, Y. Pewkliang, P. Thongsri, P. Kanjanasirirat, S. Manopwisedjaroen, S. Charoensutthivarakul, P. Wongtrakoongate, S. Pitiporn, J. Chaopreecha, S. Kongsomros, K. Jearawuttanakul, W. Wannalo, P. Khemawoot, S. Chutipongtanate, S. Borwornpinyo, A. Thititanyanont, S. Hongeng, Anti-SARS-CoV-2 activity ofandrographis paniculataExtract and its major component andrographolide in human lung epithelial cells and cytotoxicity evaluation in major organ cell representatives, J. Nat. Prod. 84 (2021) 1261–1270, https://doi.org/10.1021/acs.jnatprod.0c01324.

[44] T.H. Shi, Y.L. Huang, C.C. Chen, W.C. Pi, Y.L. Hsu, L.C. Lo, W.Y. Chen, S.L. Fu, C. H. Lin, Andrographolide and its fluorescent derivative inhibit the main proteases of 2019-nCoV and SARS-CoV through covalent linkage, Biochem. Biophys. Res. Commun. 533 (2020) 467–473, https://doi.org/10.1016/j.bbrc.2020.08.086.

[45] N.A. Murugan, C.J. Pandian, J. Jeyakanthan, Computational investigation on Andrographis paniculata phytochemicals to evaluate their potency against SARS-CoV-2 in comparison to known antiviral compounds in drug trials, J. Biomol. Struct. Dyn. 39 (2021) 4415–4426, https://doi.org/10.1080/07391102.2020.1777901.

[46] R.W.S.Kaiming Tao, Philip L. Tzou, Janin Nouhin, Hector Bonilla, Prasanna Jagannathan, SARS-CoV-2 antiviral therapy, Clin. Microbiol. Rev. 34 (2021) e00109–e00121, https://doi.org/10.1128/CMR.00109-21.

[47] M. Sasaki, K. Tabata, M. Kishimoto, Y. Itakura, H. Kobayashi, T. Ariizumi, K. Uemura, S. Toba, S. Kusakabe, Y. Maruyama, S. Iida, N. Nakajima, T. Suzuki, S. Yoshida, H. Nobori, T. Sanaki, T. Kato, T. Shishido, W.W. Hall, Y. Orba, A. Sato, H. Sawa, S-217622, a SARS-CoV-2 main protease inhibitor, decreases viral load and ameliorates COVID-19 severity in hamsters, Sci. Transl. Med. 15 (2023), eabq4064, https://doi.org/10.1126/scitranslmed.abq4064.

[48] G. Kokic, H.S. Hillen, D. Tegunov, C. Dienemann, F. Seitz, J. Schmitzova, L. Farnung, A. Siewert, C. Höbartner, P. Cramer, Mechanism of SARS-CoV-2 polymerase stalling by remdesivir, Nat. Commun. 12 (2021) 1–7, https://doi.org/10.1038/s41467-020-20542-0.

[49] F. Kabinger, C. Stiller, J. Schmitzová, C. Dienemann, G. Kokic, H.S. Hillen, C. Höbartner, P. Cramer, Mechanism of molnupiravir-induced SARS-CoV-2 mutagenesis, Nat. Struct. Mol. Biol. 28 (2021) 740–746, https://doi.org/10.1038/s41594-021-00651-0.

[50] H. Prior, H. Haworth, B. Labram, R. Roberts, A. Wolfreys, F. Sewell, Justification for species selection for pharmaceutical toxicity studies, Toxicol. Res. (Camb.). 9 (2021) 758–770, https://doi.org/10.1093/TOXRES/TFAA081.

[51] X. He, J. Li, H. Gao, F. Qiu, K. Hu, X. Cui, X. Yao, Four new andrographolide metabolites in rats, Tetrahedron 59 (2003) 6603–6607, https://doi.org/10.1016/S0040-4020(03)01053-6.

[52] H.Y. Zhao, H. Hu, Y.T. Wang, Comparative metabolism and stability of andrographolide in liver microsomes from humans, dogs and rats using ultra-performance liquid chromatography coupled with triple-quadrupole and Fourier transform ion cyclotron resonance mass spectrometry, Rapid Commun. Mass Spectrom. 27 (2013) 1385–1392, https://doi.org/10.1002/rcm.6585.

[53] M. Chen, C. Xie, L. Liu, Solubility of andrographolide in various solvents from (288.2 to 323.2) K, J. Chem. Eng. Data 55 (2010) 5297–5298, https://doi.org/10.1021/je100344z.

[54] S.M. June CH, Chimeric antigen receptor therapy, N. Engl. J. Med. 379 (2018) 64–73, https://doi.org/10.1056/NEJMra1706169.